

ON THE USE OF HIGH-ORDER FINITE DIFFERENCE SCHEMES ON OVERSET GRIDS FOR LES IN AEROACOUSTICS

F. Daude¹, T. Emmert¹, P. Lafon¹, F. Crouzet² and C. Bailly^{3,4}

¹ *LaMSID, UMR EDF/CNRS 2832, Clamart, France*

² *EDF R&D, Department of Applied Mechanics and Acoustics, Clamart, France*

³ *LMFA, ECL & UMR CNRS 5509, Ecully, France*

⁴ *IUF, France*

frederic-externe.daude@edf.fr

Abstract

This work deals with high-order finite difference schemes on overlapping grids for LES. The main numerical algorithm is based on optimized schemes and filters combined with high-order Lagrangian interpolations. This method is extended to moving grids and applied on complex fluid/acoustic phenomena in a ducted cavity.

1 Introduction

The need for high-order methods, as summarized by Colonius and Lele (2004), is recognized for performing accurate simulations of various physical phenomena, including direct numerical (DNS) and large-eddy (LES) simulations of turbulence, computational aeroacoustics (CAA) and fluid/structure interactions (FSI). We focus herein on the direct noise computation (DNC) based on compressible LES for the prediction of aeroacoustic phenomena on complex configurations. The explicit optimized finite-difference schemes, e.g. Tam and Webb (1993) and Bogey and Bailly (2004), are an efficient and attractive way to provide low dispersive and low dissipative methods. However, these procedures, in most early works, were limited to academic cases with single domain and Cartesian grids. With the use of general curvilinear coordinates transformation, see Visbal and Gaitonde (2002) and Marsden *et al.* (2005), these methods can now be applied on more complex geometries. In the same way, high-order overset-grid approaches, e.g. Delfs (2001) and Sherer and Scott (2005), are developed to handle realistic configurations including multiple bodies. Another advantage of the overset-grid strategy is the use of multi-block meshes which can be used on massively parallel computing platforms. In addition, overset-grid approach makes it possible to deal with moving bodies via preventing large mesh deformations. After briefly presenting the governing equations and the algorithm retained on overlapping grids, a classical example of validation is detailed.

Then, the extension to moving grids is studied. Finally, the overlapping grids are used to compute the noise generated by a ducted cavity.

2 Governing equations

The filtered unsteady compressible Navier-Stokes equations are expressed in general time-dependent curvilinear coordinates:

$$\partial_\tau \left(\frac{1}{J} U \right) + \partial_\xi \hat{E} + \partial_\eta \hat{F} + \partial_\zeta \hat{G} = \hat{S}^\nu + \hat{S}^{\nu_{\text{sgs}}} \quad (1)$$

with U the filtered conservative variables vector, J the Jacobian of the geometric transformation between the physical (x, y, z, t) and the computational (ξ, η, ζ, τ) domains, \hat{E} , \hat{F} and \hat{G} the inviscid flux-vectors, \hat{S}^ν the source term from the viscous flux-vectors and $\hat{S}^{\nu_{\text{sgs}}}$ the corresponding subgrid scale source term. The LES strategy in the present work is the same as in Bogey and Bailly (2006). The dissipative effects of the subgrid scales are taken into account through the high-order selective filter presented in the following section. In the same time, the interactions between the resolved and the non-resolved scales are neglected: $\hat{S}^{\nu_{\text{sgs}}} = 0$. The expression of inviscid and viscous flux-vectors are given in Visbal and Gaitonde (2002). In addition, with the use of finite-difference schemes, the following metrics relations must be satisfied:

$$\left\{ \begin{array}{l} \partial_\xi \hat{\xi}_x + \partial_\eta \hat{\eta}_x + \partial_\zeta \hat{\zeta}_x = 0 \\ \partial_\xi \hat{\xi}_y + \partial_\eta \hat{\eta}_y + \partial_\zeta \hat{\zeta}_y = 0 \\ \partial_\xi \hat{\xi}_z + \partial_\eta \hat{\eta}_z + \partial_\zeta \hat{\zeta}_z = 0 \\ \partial_\tau (1/J) + \partial_\xi \hat{\xi}_t + \partial_\eta \hat{\eta}_t + \partial_\zeta \hat{\zeta}_t = 0 \end{array} \right. \quad (2)$$

where $\hat{\xi}_x, \hat{\eta}_x, \hat{\zeta}_x, \hat{\xi}_y, \hat{\eta}_y, \hat{\zeta}_y, \hat{\xi}_z, \hat{\eta}_z, \hat{\zeta}_z$ are the spatial metrics and $\hat{\xi}_t, \hat{\eta}_t, \hat{\zeta}_t$ are the temporal metrics. The last relation known in the literature as the Geometric Conservation Law (GCL), refer to Thomas and Lombard (1979), only concerns moving and deforming meshes computations.

3 Numerical procedure on fixed grids

For interior points, first spatial derivatives in Equation (1) are discretized by the optimized centered 11-point finite-difference scheme in conjunction with the optimized explicit 11-point low-pass filter of Bogey and Bailly (2004), to remove grid-to-grid oscillations. The time integration is performed via a standard explicit fourth-order low-storage Runge-Kutta scheme denoted RK4 in the following. In addition, in regions with strong shocks, a non-linear shock-capturing filter is applied after each time step, e.g. Emmert (2007) and Daude *et al.* (2008). This filter is based on the adaptive non-linear artificial dissipation model proposed in Kim and Lee (2001). Furthermore, a modified Jameson sensor has been proposed to determine the shock location.

In order to preserve the low-dissipation and low-dispersion properties of the algorithm near the wall boundaries, the optimized 11-points non-centered finite difference schemes proposed by Berland *et al.* (2007) are used. As the corresponding non-centered filters exhibit stability problems, centered filters on smaller stencils can be optionally applied at wall boundaries. Moreover, two kinds of non-reflective boundary conditions are used: the characteristics proposed by Thompson (1990) and the 3D far-field radiation conditions generalized by Bogey and Bailly (2002).

According to Visbal and Gaitonde (2002), in order to satisfy the metric error cancellation, the spatial metrics are expressed using the conservative form proposed by Thomas and Lombard (1979):

$$\begin{cases} \hat{\xi}_x &= (y_\eta z)_\zeta - (y_\zeta z)_\eta \\ \hat{\eta}_x &= (y_\zeta z)_\xi - (y_\xi z)_\zeta \\ \hat{\zeta}_x &= (y_\xi z)_\eta - (y_\eta z)_\xi \end{cases} \quad (3)$$

In order to address complex geometric configurations, an overset-grid technique is retained. This overset-grid approach is also used as a domain decomposition procedure for the implementation of the algorithm on massively parallel machines. Following the work of Sherer and Scott (2005), a high-order, explicit non-optimized Lagrangian method is used to perform the communication between the non-coincident overlapping grids. Finally, eighth-order Lagrangian polynomials have been assessed to be a good compromise between accuracy and efficiency, e.g. Emmert (2007). In practice, the present algorithm has been interfaced with the freely available *Overture* library developed by the Lawrence Livermore National Laboratory, see Henshaw (1998).

4 Noise radiated by the flow around a cylinder

A 2D flow past a cylinder at low Reynolds and Mach numbers ($Re_D = 150$ and $M_\infty = 0.33$) is computed with overlapping grids (see Fig. 1). Results are

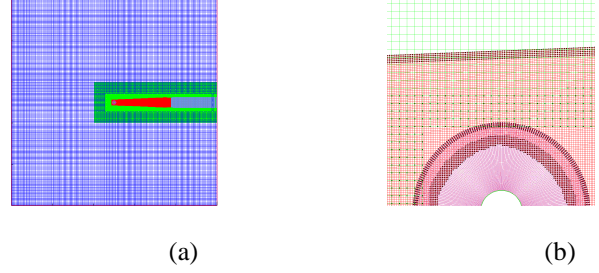


Figure 1: Noise radiated by the flow around the cylinder: (a) global view of the overlapping grids of the computational domain composed of 5 component grids; (b) detailed view around the cylinder region

identical to the ones computed with a unique circular mesh, e.g. Emmert (2007). The dipole character-

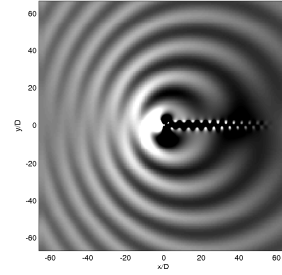


Figure 2: Instantaneous pressure fluctuation field.

istic of the noise source and the von Kármán vortex street are retrieved (see Fig. 2). More complex configurations with industrial relevance are studied using this high-order algorithm on overlapping grids such as sudden expansion in Emmert *et al.* (2007 a).

5 Numerical procedure on moving grids

The algorithm is now extended to moving and deforming grids. In this case, a special attention must be paid on the metric evaluation procedures to satisfy the GCL (2) as mentioned by Visbal and Gaitonde (2002) and by Hixon (2000). The approach used in the present work is based on work by Visbal and Gaitonde (2002) where the time derivative in Equation (1) is splitted into two parts:

$$\partial_\tau \left(\frac{1}{J} U \right) = \frac{1}{J} \partial_\tau U + U \partial_\tau \left(\frac{1}{J} \right) \quad (4)$$

The second term of the right-hand side of Equation (4) is then evaluated using the GCL relation. Finally, the equations resolved using the algorithm can be expressed as:

$$\partial_\tau U + J \left[\partial_\xi \hat{E} + \partial_\eta \hat{F} + \partial_\zeta \hat{G} - \hat{S}^\nu - U \left(\partial_\xi \hat{\xi}_t + \partial_\eta \hat{\eta}_t + \partial_\zeta \hat{\zeta}_t \right) \right] = 0 \quad (5)$$

The stability requirement is modified due to the mesh movement and becomes more restrictive. The spatial metrics are still evaluated following Equation (3). The temporal metrics are expressed using the mesh velocity $\vec{V}_e = (x_\tau, y_\tau, z_\tau)^T$ as in Visbal and Gaitonde (2002):

$$\begin{cases} \hat{\xi}_t = -\left(x_\tau \hat{\xi}_x + y_\tau \hat{\xi}_y + z_\tau \hat{\xi}_z\right) \\ \hat{\eta}_t = -\left(x_\tau \hat{\eta}_x + y_\tau \hat{\eta}_y + z_\tau \hat{\eta}_z\right) \\ \hat{\zeta}_t = -\left(x_\tau \hat{\zeta}_x + y_\tau \hat{\zeta}_y + z_\tau \hat{\zeta}_z\right) \end{cases} \quad (6)$$

Note that this formulation is similar to the classical ALE (Arbitrary Lagrangian Eulerian) expression in a finite-volume framework. In the present work, in order to ensure the time consistency between grid and flow, we update the grid coordinates in the same time as the flow variables via the RK4 scheme:

$$x_{i,j,k}^{(l)} = x_{i,j,k}^n + \Delta\tau \beta^{(l)} (x_\tau)_{i,j,k}^{(l-1)} \quad (7)$$

with $x^{(0)} = x^n$, $x^{n+1} = x^{(4)}$, $\Delta\tau$ the time step and $\beta^{(l)}$ the Runge-Kutta coefficients.

With the presence of moving bodies, the relative position of the overlapping grids changes continuously during the flow simulation. Thus, the interpolation stencils, the holes cut by the overset-grid approach and the Lagrangian coefficients must be recomputed at each RK4 stage. The overset-grid strategy is a powerful tool for the simulation of flows with one or multiple moving bodies, since the grids do not have to be regenerated as the solution evolves. Only the interpolation data used to communicate information between the grids are updated. In practice, the overlapping grid generator *Ogen*, refer to Henshaw (1998), is called at each stage of the RK4 scheme to update the interpolation stencils and holes.

6 Validation on simple moving/deforming grids problems

The validation on moving/deforming problems is performed in two steps. First, we consider a single domain in order to only assess the algorithm and the time metrics evaluation without the overset-grid considerations. Second, a simple multi-domain computation with moving overlapping meshes is performed. Only inviscid problems are considered here because the grids movement only modifies the inviscid flux-vectors.

Inviscid vortex advection on a deforming mesh

We consider the vortex advection on a dynamically deforming 2-D mesh. The computational domain is taken as $[-2, 2] \times [-1, 1]$ and periodic conditions are used for the four boundaries. Initially, an uniform mesh is retained with $\Delta x_0 = \Delta y_0 = 1/100$. The

mesh velocity is analytically specified by the equation:

$$\begin{cases} (x_\tau)_{i,j} = \alpha_x \sin\left(n_x \pi \frac{y_{i,j}(0) - y_{\min}}{y_{\max} - y_{\min}}\right) \\ (y_\tau)_{i,j} = \alpha_y \sin\left(n_y \pi \frac{x_{i,j}(0) - x_{\min}}{x_{\max} - x_{\min}}\right) \end{cases} \quad (8)$$

with

$$\begin{cases} \alpha_x = 2\pi\omega A_x \Delta x_0 \cos(2\pi\omega t) \exp(R) \\ \alpha_y = 2\pi\omega A_y \Delta y_0 \cos(2\pi\omega t) \exp(R) \\ R = -4 \log(2) \frac{x_{i,j}(0)^2 + y_{i,j}(0)^2}{(y_{\max} - y_{\min})^2} \end{cases}$$

The mesh velocity is assumed constant during a time iteration. The different parameters are: $A_x = A_y = 2$, $n_x = n_y = 6$, $x_{\min} = y_{\min} = -0.5$, $x_{\max} = y_{\max} = 0.5$ and $\omega = 2$. A similar test case is presented in Visbal and Gaitonde (2002).

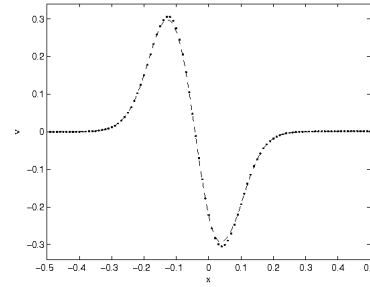


Figure 3: Effect of the mesh dynamic deformation on the swirl velocity: . static case ; - - deforming case

Two computations are performed, one on a static grid which is the initial uniform grid and the other with the grid velocity expressed in Equation (8), with $CFL = 0.5$ designed with the initial non deformed grid. The vortex is initially placed on $(x_c, y_c) = (0, 0)$ and results are visualized when it returns at its initial position. The swirl velocity profiles at $y = 0$ in the static and deforming cases plotted on Fig. 3 are similar which shows that it is possible to preserve the high-order schemes properties on dynamically deforming meshes.

Cylinder advection in an inviscid uniform flow

The second test case is an advection of a cylinder in an uniform flow with no velocity. The computational domain is taken as $[-2, 2] \times [-2, 2]$, and is divided in two grids: a fixed Cartesian one with an uniform mesh of step size $\Delta x = \Delta y = 1/50$ and a moving cylindrical one. This mesh is plotted on Fig. 4. Initially, the center of the cylinder is located at $x_c = 0.85$. A constant displacement of the cylindrical domain is imposed at every time step: $d = 0.04\Delta x$. Then, the mesh velocity is computed using the relation $x^{(l+1)} - x^{(l)} =$

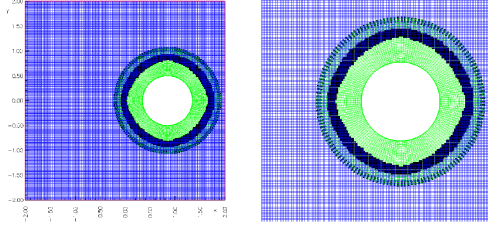


Figure 4: Cylinder advection ; View of the overlapping grids: the interpolation points of the two domains in black

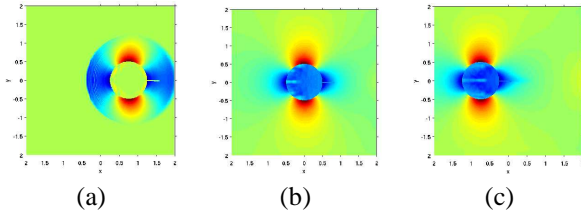


Figure 5: Cylinder advection ; Velocity field: (a) at $x_c = 0.75$; (b) at $x_c = 0$; (c) at $x_c = 0.75$

$d/4$ for every stage of the RK4 scheme. The computation is performed with $CFL = 0.5$. The velocity field of the inviscid flow over an moving cylinder is plotted on Fig. 5 for three different positions. First, a transient acoustic wave is generated by the initial motion of the cylinder. Then, the wave leaves the computational domain and a symmetric stationary solution with respect to the cylinder is reached.

7 LES of the flow past a ducted cavity

To underline the capacities of our high-order algorithm on overlapping grids, a LES of the flow at moderate Mach number past a ducted cavity is performed in the following of Emmert *et al.* (2007 b).

Motivation and precedent works

It is well established that compressible flows past open cavities cause high levels of pressure fluctuations. Many experimental and numerical investigations were performed to understand the underlying physical mechanism and develop efficient control strategy, see Rowley and Williams (2006) for a review. The self-sustained cavity oscillations are due to a complex feedback mechanism between the upstream and downstream corners which can be described as follows. Vortices in the shear layer interact with the downstream corner of the cavity and generate pressure disturbances, which propagate upstream and create new instabilities in the shear layer. This feedback mechanism is referred as cavity (or Rossiter) modes (RM) which frequencies can be given by the semi-

empirical formula, proposed by Rossiter (1964):

$$St_R = \frac{f_{n_R} d}{U} = \frac{n_R - \alpha}{M + 1/\kappa} \quad (9)$$

in which U and M are the external flow velocity and Mach number respectively, d is the cavity length, n_R is the mode number. The two empirical constants α and κ are linked to the delay between the vortex impact and the acoustic wave emission and the convection velocity of vortices in the shear layer. For open cavities, the self-sustained oscillations remain weak at low Mach numbers. This is the reason why the studies encountered in the literature mainly concerns high-speed flows, e.g. Gloerfelt *et al.* (2003) and Larchevêque *et al.* (2003). Developing effective control strategy and understanding the underlying physical mechanism of the cavity noise reduction is still a research area, refer to Rowley and Williams (2006), Stanek *et al.* (2007) and Comte *et al.* (2008).

In contrast, for ducted cavities, the possible lock-in between cavity modes and duct acoustic modes can lead to high amplitude oscillations even at low speed. Such configurations can be found in pipe systems with flow control devices such as valves, in organ pipes or in flutes, for instance. The tonal cavity noise can also excite the acoustic modes of the pipes. The frequencies of the duct transverse resonance (DM) are given by:

$$St_D = \frac{f_{n_D} d}{U} = \frac{n_D d}{2HM} \quad (10)$$

in which H is the height of the duct and n_D is the mode number. The ducted cavity considered here is

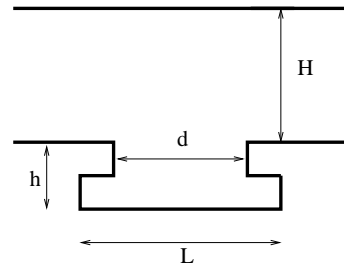


Figure 6: Ducted cavity: sketch of the geometry; $d = 0.05$ m, $h = 0.02$ m, $H = 0.137$ m, $L = 0.073$ m.

partially covered as shown in Fig. 6. This geometry where $d = 0.05$ m, $h = 0.02$ m, $H = 0.137$ m, and $L = 0.073$ m has been studied previously, e.g. Lafon *et al.* (2003) and Emmert *et al.* (2007 b). For this configuration, RMs are given with $\alpha = 0.25$ and $1/\kappa = 0.57$ in Equation (9). Experiments give the following results: lock-in occurs at $M = 0.13$ between RM3 and DM1, at $M = 0.18$ between RM2 and DM1 and at $M = 0.23$ between RM3 and DM2. In Lafon *et al.* (2003), a 2-D numerical solution has been obtained using a second-order TVD-Euler code and compared with experimental measurements. Even

if RMs were retrieved, turbulent aspects could not be considered. A LES have been carried out in Emmert *et al.* (2007 b) by using coincident grids. The lock-in phenomenon has been retrieved and the frequencies has been well estimated. However the amplitude of RMs was not well resolved. The overset-grid strategy is retained here to refine the mesh in sensitive zones as the shear layer where fine turbulent fluctuations can play a crucial role.

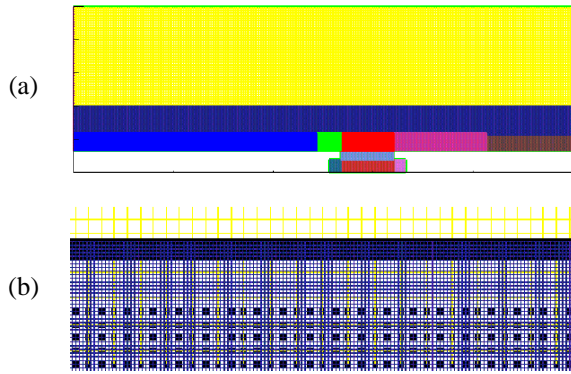


Figure 7: Ducted cavity: (a) view of the eleven component grids, (b) zoom in the overset region.

Computational set up

The mesh is generated by *Ogen* and displayed in Figure 7. It consists of eleven component grids. The grid spacing is kept constant in the cavity and in the boundary layer ($\Delta x = 1.4 \times 10^{-4}$ m, $\Delta y = 1 \times 10^{-4}$ m). An intermediate grid is used between this region and the duct. In the duct, a grid adapted to acoustic is designed. Finally, the number of cells is multiplied by a factor of 10 compare to Emmert *et al.* (2007 b). In the precedent study, the inflow boundary profile was imposed from the inlet to the upstream corner of the cavity. In this work, this boundary layer is left free to evolve at a distance before the upstream corner. This is done in order to try to better catch the interactions between the shear layer and the incoming boundary layer. Then, only fluctuations are filtered to prevent excessive damping and a sponge zone is used to avoid spurious reflections.

Analysis of results

Figures 8, 9 and 10 show the instantaneous pressure field in the duct and spanwise average vorticity modulus in the cavity obtained by LES for $M = 0.13$, $M = 18$ and $M = 0.23$. At $M = 0.13$, the lock-in between RM3 and DM1 is well retrieved since three vortices are present in the shear layer. This lock-in seems to be more evident than in Emmert *et al.* (2007 b). At $M = 0.18$, the lock-in between RM2, two vortices in the shear layer, and DM1 is also retrieved. At $M = 0.23$, the lock-in between RM3, three vortices in the shear layer, and DM2 is less matched, but appears in a more evident way than in Emmert *et al.* (2007 b).

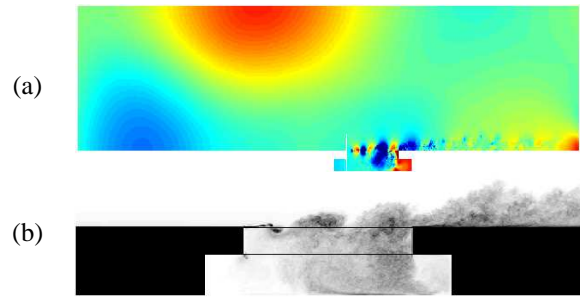


Figure 8: Ducted cavity at $M = 0.13$; instantaneous results: (a) pressure fluctuations in the duct (< 100 Pa), (b) spanwise average vorticity modulus in the cavity

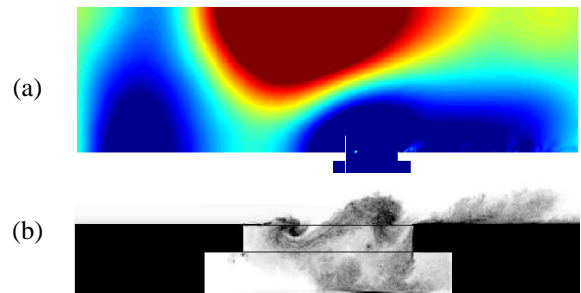


Figure 9: Ducted cavity at $M = 0.18$; instantaneous results: (a) pressure fluctuations in the duct (< 100 Pa), (b) spanwise average vorticity modulus in the cavity

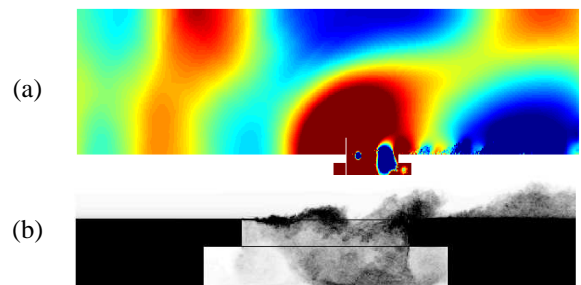


Figure 10: Ducted cavity at $M = 0.23$; instantaneous results: (a) pressure fluctuations in the duct (< 100 Pa), (b) spanwise average vorticity modulus in the cavity

More details concerning the coupling phenomena are available in Emmert *et al.* (2008).

8 Conclusions and future work

A high-order algorithm with overlapping grids suitable for noise and flow computations is extended on moving/deforming grids problems. The validation procedure is performed on 2-D inviscid test cases. The grid dynamic motion does not damage the scheme properties. Finally, the overset-grid approach makes it possible to perform a realistic LES of a confined cavity flow via a better capture of the turbulent structures developing in the shear layer.

Further analysis based on better converged turbulent statistics are in progress. Future efforts will focus on the extension of the moving overset-grid approach on 3-D turbulent flows interacting with moving bodies as involved in aeroelasticity problems.

Acknowledgments

This work is supported by the “Agence Nationale de la Recherche” under the reference ANR-06-CIS6-011. The authors want to thank Dr. Bill Henshaw for his useful advices concerning the overset strategy.

References

- Berland J., Bogey C., Marsden O., and Bailly, C. (2007), High-order, low dispersive and low dissipative explicit schemes for multiple-scale and boundary problems *J. Comp. Phys.*, Vol. 224, pp. 637-662.
- Bogey, C. and Bailly, C. (2002), Three-dimensional non-reflective boundary conditions for acoustic simulations: far field formulation and validation test cases, *Acta Acustica*, Vol. 88, pp. 463-471.
- Bogey, C. and Bailly, C. (2004), A family of low dispersive and low dissipative explicit schemes for flow and noise computations, *J. Comp. Phys.*, Vol. 194, pp. 194-214.
- Bogey, C. and Bailly, C. (2006), Large eddy simulations of transitional round jets: influence of the Reynolds number on flow development and energy dissipation, *Phys. of Fluids*, Vol. 213, pp. 777-802.
- Comte P., Daude F., and Mary, I. (2008), Simulation of the reduction of the unsteadiness in a passively-controlled transonic cavity flow, submitted to *J. Fluids Struct.*
- Colonus, T. and Lele, S.K. (2004), Computational aeroacoustics: progress on nonlinear problems on sound generation, *Prog. Aerospace Sci.*, Vol. 40, pp. 345-416.
- Daude F., Emmert T., Lafon P., Crouzet F., and Bailly, C. (2008), A high-order algorithm for compressible LES in CAA applications, AIAA Paper 08-3049.
- Delfs, J.W. (2001) An overlapped grid technique for high resolution CAA schemes for complex geometries, AIAA 01-2199.
- Emmert T. (2007), Development of a multidomain high-order algorithm for computational aeroacoustics: application to subsonic and transonic confined flows, *PhD thesis*, École Centrale de Lyon
- Emmert T., Lafon P., and Bailly, C. (2007 a), Computation of Aeroacoustic Phenomena in Subsonic and Transonic Ducted Flow, AIAA Paper 07-3429.
- Emmert T., Lafon P., and Bailly, C. (2007 b), Numerical simulation of the flow over a confined shallow cavity, TSFP5.
- Emmert T., Lafon P., and Bailly, C. (2008), Numerical study of aeroacoustic coupling in a subsonic confined cavity, AIAA Paper 08-2848.
- Gloerfelt X., Bogey C., and Bailly, C. (2003), Numerical evidence of mode switching in the flow-induced oscillations by a cavity, *International Journal of Aeroacoustics*, Vol. 2, pp. 193-217.
- Henshaw W.D. (1998), Ogen : An Overlapping Grid Generator for Overture, Lawrence Livermore National Laboratory, UCRL-MA-132237.
- Hixon R. (2000), Numerically Consistent Strong Conservation Grid Motion for Finite Difference Schemes, *AIAA J.*, Vol. 38, pp. 1586-1593.
- Kim, J.W. and Lee, D.J. (2001), Adaptive Nonlinear Artificial Dissipation Model for Computational Aeroacoustics, *AIAA J.*, Vol. 39, pp. 810-818.
- Lafon P., Caillaud S., Devos J. P., and Lambert, C. (2003), Aeroacoustical coupling in a ducted shallow cavity and fluid/structure effects on a steam line, *J. Fluids Struct.*, Vol. 18, pp 695-713.
- Larchevêque L., Sagaut P., Mary I., Labbe O. and Comte, P. (2003), Large eddy simulation of a compressible flow past a deep cavity, *Phys. of Fluids*, Vol. 15, pp. 193-210.
- Marsden O., Bogey C. and Bailly, C. (2005), High-order curvilinear simulations of flows around non-Cartesian bodies, *J. Comput. Acoust.*, Vol. 13, pp. 731-748.
- Rossiter J.E. (1964), Wind-tunnel experiments on the flow over rectangular cavities at subsonic and transonic speeds, *Aeronautical Research Council Reports and Emoranda*, 3438.
- Rowley, C.W. and Williams, D.R. (2006), Dynamics and control of high-Reynolds number flow over open cavities, *Annu. Rev. Fluid Mech.*, Vol. 30, pp. 251-276.
- Sherer, S.E. and Scott, J.N. (2005), High-order compact finite-difference methods on general overset grids, *J. Comp. Phys.*, Vol. 210, pp. 459-496.
- Stanek M.J., Visbal M.R., Rizzetta D.P., Rubin S.G. and Khosla P.K. (2007), On a mechanism of stabilizing turbulent free shear layer in cavity flows, *Comput. Fluids*, Vol. 36, pp. 1621-1637.
- Tam, C.K.W. and Webb, J.C. (1993), Dispersion-Relation-Preserving Finite Differences Schemes for Computational Acoustics, *J. Comp. Phys.*, Vol. 107, pp. 262-281.
- Thomas, P.D. and Lombard, C.K. (1979), Geometric conservation law and its application to flow computations on moving grids, *AIAA J.*, Vol. 17, pp. 1030-.
- Thompson, K. W. (1990), Time dependent boundary conditions for hyperbolic systems, II, *J. Comp. Phys.*, Vol. 89, pp. 439-461.
- Visbal, M.R. and Gaitonde, D.V. (2002), On the Use of Higher-Order Finite-Difference Schemes on Curvilinear and Deforming Meshes, *J. Comp. Phys.*, Vol. 181, pp. 155-185.